ReITR: Relation Transformer for Scene Graph Generation

Yuren Cong, Michael Ying Yang, and Bodo Rosenhahn

Abstract—Different objects in the same scene are more or less related to each other, but only a limited number of these relationships are noteworthy. Inspired by DETR, which excels in object detection, we view scene graph generation as a set prediction problem and propose an end-to-end scene graph generation model ReITR which has an encoder-decoder architecture. The encoder reasons about the visual feature context while the decoder infers a fixed-size set of triplets subject-predicate-object using different types of attention mechanisms with coupled subject and object queries. We design a set prediction loss performing the matching between the ground truth and predicted triplets for the end-to-end training. In contrast to most existing scene graph generation methods, ReITR is a one-stage method that predicts a set of relationships directly only using visual appearance without combining entities and labeling all possible predicates. Extensive experiments on the Visual Genome and Open Images V6 datasets demonstrate the superior performance and fast inference of our model.

Index Terms—Scene Understanding, Scene Graph Generation, One-Stage, Visual Relationship Detection

◆

1 INTRODUCTION

IN scene understanding, a scene graph is a graph structure whose nodes are the entities that appear in the image and whose edges represent the relationships between entities [1]. Scene graph generation (SGG) is a semantic understanding task that goes beyond object detection and is closely linked to visual relationship detection [2]. At present, scene graphs have shown their potential in different vision-language tasks such as image retrieval [1], image captioning [3], [4], visual question answering (VQA) [5] and image generation [6], [7]. The task of scene graph generation has also received sustained attention in the computer vision community. Most existing methods for generating scene graphs employ an object detector (e.g. FasterRCNN [8]) and use some specific neural networks to infer the relationships. The object detector generates proposals in the first stage, and the relationship classifier labels the edges between the object proposals for the second stage. Although these two-stage approaches have made incredible progress, they still suffer from the drawback that these models require a large number of trained parameters. Moreover, if n object proposals are given, the relationship inference network runs the risk of learning based on erroneous features provided by the detection backbone and has to predict $O(n^2)$ relationships, which leads to slow inference. Many previous works [9], [10], [11], [12], [13] have integrated semantic knowledge to improve their performance. However, these models face significant biases in relationship inference conditional on subject and object categories. They prefer to predict the predicates that are popular between particular subjects and objects, rather than those based on visual appearance.

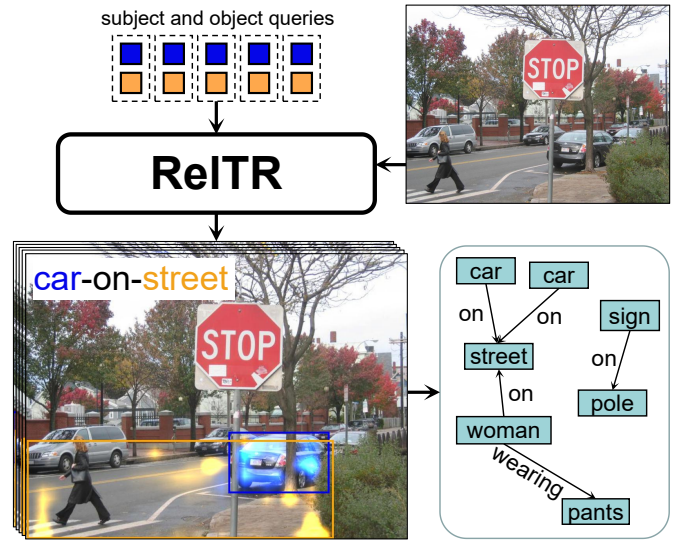Recently, the one-stage models have emerged in the field

Fig. 1: ReITR can predict the subjects (blue), objects (orange) and their predicates simultaneously with learned subject and object queries. For the specific relationship `<car-on-street>`, ReITR attends to the region adjacent to the car and street.

of object detection [14], [15], [16], [17]. They are attractive for the fast speed, low costs and simplicity. These are also the properties that are urgently needed for the scene graph generation models. Detection Transformer (DETR) [18] views object detection as an end-to-end set prediction task and proposes a set-based loss via bipartite matching. This strategy can be extended to scene graph generation: based on a set of learned subject and object queries, a fixed number of triplets `<subject-predicate-object>` could be predicted by reasoning about the global image context and co-occurrences of entities. However, it is challenging to im-

---

- *Yuren Cong and Bodo Rosenhahn are with Institute of Information Processing, Leibniz University Hannover, Germany. E-mail: {cong, rosenhahn}@tnt.uni-hannover.de.*
- *Micheal Ying Yang is with Scene Understanding Group, University of Twente, The Netherlands. Email: michael.yang@utwente.nl.*

plement such an intuitive idea. The model needs to predict both the location and the category of the subject and object, and also consider their semantic connection. Furthermore, the direct bipartite matching is not competent to assign ground truth information to relationship predictions. This paper aims to address these challenges.

We propose a novel end-to-end framework for scene graph generation, named **Relation Transformer (RelTR)** [1]. As shown in Fig. 1, RelTR attends to the corresponding regions of interest for different relationships and predicts subjects, objects, and their predicates concurrently. We evaluate RelTR on Visual Genome [19] and large-scale Open Images V6 [20]. The **main contributions** of this work are summarized as follows:

- Different from most existing advanced approaches that classify the dense relationships between all entity proposals from the object detection backbone, our one-stage method can generate a sparse scene graph by decoding the visual appearance with the subject and object queries learned from the data.
- RelTR generates scene graphs based on visual appearance only, which has fewer parameters and faster inference compared to other SGG models while having competitive performance.
- A set prediction loss is designed to perform the matching between the ground truth and predicted triplets with an IoU-based assignment strategy.
- With the decoupled entity attention, the triplet decoder of RelTR can improve the localization and classification of subjects and objects with the entity detection results from the entity decoder.
- Through comprehensive experiments, we explore which components are critical for the performance and analyze the working mechanism of learned subject and object queries.

The remainder of the paper is structured as follows. In Section 2, we review related work in scene graph generation. Section 3 presents our proposed method. Experimental results of the proposed framework are discussed in Section 4. Section 5 concludes this paper.

2 RELATED WORK

2.1 Scene Graph Generation

Scene graphs have been proposed in [1] for the task of image retrieval and attract increasing attention in computer vision and natural language processing communities for different scene understanding tasks such as image captioning [21], [22], [23], VQA [24], [25], [26] and image synthesis [27], [28], [29]. The main purpose of scene graph generation (SGG) is to detect the relationships between objects in the scene. Many earlier works were limited to identifying specific types of relationships such as spatial relationships between entities [30], [31]. The universal visual relationship detection is introduced in [2]. Their inference framework, which first detects entities in an image first and then determines dense relationships, was widely adopted in subsequent works, including their evaluation settings and metrics as well.

Now many models [32], [33], [34], [35], [36], [37] are available to generate scene graphs from different perspectives, and some works even extend the scene graph generation task from images to videos [38], [39], [40], [41]. Two-stage methods following [2] are currently dominating scene graph generation: several works [9], [32], [42], [43] use residual neural networks with the global context to improve the quality of the generated scene graphs. Xu *et al.* [42] use standard RNNs to iteratively improves the relationship prediction via message passing while MotifNet [9] stacks LSTMs to reason about the local and global context. Graph-based models [44], [45], [46], [47], [48] perform message passing and demonstrate good results. Factorizable Net [45] decomposes and combines the graphs to infer the relationships. The attention mechanism is integrated into different types of graph-based models such as Graph R-CNN [44], GPI [49] and ARN [50]. With the rise of Transformer [51], there are several attempts using Transformer to detect visual relationships and generate scene graphs in very recent works [36], [52], [53]. To improve the performance, many works are no longer limited to using only visual appearance. Semantic knowledge can be utilized as an additional feature to infer scene graphs [2], [9], [11], [54], [55]. Furthermore, statistic priors and knowledge graphs have been introduced in [11], [56], [57], [58], [59].

Compared to the boom of two-stage approaches, one-stage approaches are still in their infancy and have the advantage of being simple, fast and easy to train. To the best of our knowledge, FCSGG [60] is currently the only one-stage scene graph generation framework that encodes objects as box center points and relationships as 2D vector fields. While FCSGG model being lightweight and fast speed, it has a significant performance gap compared to other two-stage methods. To fill this gap, we propose Transformer-based RelTR using only visual appearance in this work with fewer parameters, faster inference speed, and higher accuracy. Distinct from the other two-stage Transformer-based approaches [36], [52], [53] that utilize the attention mechanism to capture the context of the entity proposals from an object detector, RelTR can decode the global feature maps directly with the subject and object queries learned from the data to generate a sparse scene graph.

2.2 Transformer and Set Prediction

The original Transformer architecture was proposed in [51] for sequence transduction. Its encoder-decoder configuration and attention mechanism are also used to solve various computer vision tasks in different ways, e.g. object detection [18], human-object interaction (HOI) detection [61], and dynamic scene graph generation [39].

DETR [18] is a seminal work based on Transformer architecture for object detection in recent years. It views detection as a set prediction problem. In the end-to-end training, with the object queries, DETR predicts a fixed-size set of object proposals and performs a bipartite matching between proposals and ground truth objects for the loss function. This concept of query-based set prediction quickly gains popularity in the computer vision community. Many tasks can be reformulated as set prediction problems, e.g. instance segmentation [62], image captioning [63] and multiple-

---

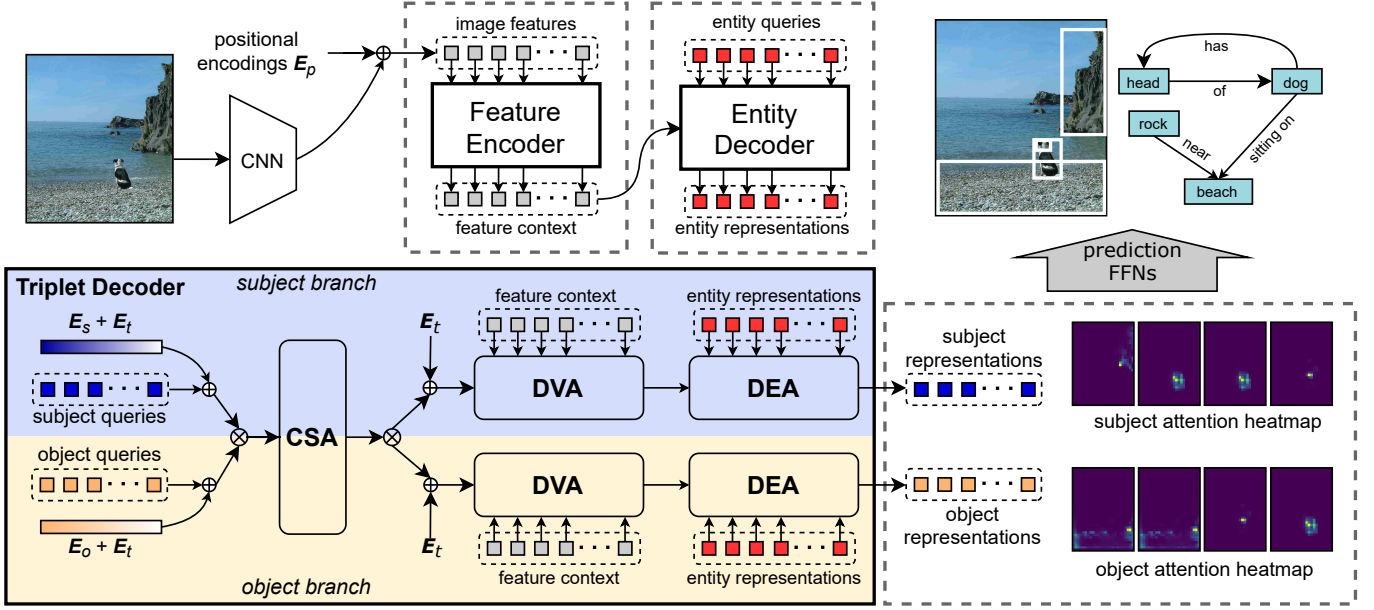1. The source code is made publicly available on Github.

Fig. 2: Given a set of learned subject and object queries coupled by subject and object encodings, RelTR captures the dependencies between relationships and reasons about the feature context and entity representations, respectively the output of the feature encoder and entity decoder, to directly compute a set of subject and object representations. A pair of subject and object representations with attention heat maps is decoded into a triplet `<subject-predicate-object>` by feed forward networks (FFNs). **CSA**, **DVA** and **DEA** stand for Coupled Self-Attention, Decoupled Visual Attention and Decoupled Entity Attention. E_p, E_t, E_s and E_o are the positional, triplet, subject and object encodings respectively. $\oplus$ indicates element-wise addition, while $\otimes$ indicates concatenation or split.

object tracking [64]. Some works [65], [66] attempt to further improve object detection based on DETR.

HOI detection localizes and recognizes the relationships between humans and objects, whose result is a sub-graph of the scene graph. Several HOI detection frameworks [61], [67] have been developed that use holistic triplet queries to directly infer a set of interactions. However, such concept is difficult to be generalized to the more complex task of scene graph generation. On large-scale datasets, such as Visual Genome [19] and Open Images [20], localization and classification of subjects and objects using only triplet queries may likely result in low accuracy. On the contrary, our proposed RelTR predicts the general relationships using coupled subject and object queries to achieve high accuracy.

3 METHOD

A scene graph $\mathcal{G}$ consists of entity vertices $\mathcal{V}$ and relationship edges $\mathcal{E}$. Different from previous works detecting a set of entity vertices and labeling the predicates between the vertices, we propose a one-stage model, Relation Transformer (RelTR), to directly predict a fixed-size set of $< \mathcal{V}_{sub} - \mathcal{E}_{prd} - \mathcal{V}_{obj} >$ for scene graph generation.

3.1 Preliminaries

3.1.1 Transformer

We provide a brief review on Transformer and its attention mechanism. Transformer [51] has an encoder-decoder structure and consists of stacked attention functions. The input of a single-head attention is formed from queries Q, keys K and values V while the output is computed as:

$$Attention(Q, K, V) = softmax\left(\frac{QK^T}{\sqrt{d_k}}\right)V, \qquad (1)$$

where d_k is the dimension of K. In order to benefit from the information in different representation sub-spaces, multi-head attention is applied in Transformer. A complete attention function is a multi-head attention followed by a normalization layer with residual connection and denoted as $Att(.)$ in this paper for simplicity.

3.1.2 DETR

This entity detection framework [18] is built upon the standard Transformer encoder-decoder architecture. First, a CNN backbone generates a feature map $Z_0 \in \mathbb{R}^{H \times W \times d}$ for an image. With the self-attention mechanism, the encoder computes a new feature context $Z \in \mathbb{R}^{HW \times d}$ using the flatted Z_0 and fixed positional encodings $E_p \in \mathbb{R}^{HW \times d}$. The decoder transforms N_e entity queries into the entity representations $Q_e \in \mathbb{R}^{N_e \times d}$. The entity queries interact with each other to capture the entity context and extract visual features from Z.

For the end-to-end training, a set prediction loss for entity detection is proposed in DETR by assigning the ground truth entities to predictions. The ground truth set of size N_e is padded with ϕ `<background>`, and a cost function $c_m(\hat{y}, y)$ is applied to compute the matching cost between a prediction $\hat{y}$ and ground truth entity $y = \{c, b\}$ where c, b indicates the target class and box coordinates respectively. Given the cost matrix C_{ent}, the entity prediction-ground truth assignment is computed with the Hungarian

algorithm [68]. The set prediction loss for entity detection can be presented as:

$$L_{entity} = \sum_{i=1}^{N_e} \left[L_{cls} + \mathbb{1}_{\{c^i \neq \phi\}} L_{box} \right], \tag{2}$$

where L_{cls} denotes the cross-entropy loss for label classification and $c^i \neq \phi$ means that `<background>` is not assigned to the i-th entity prediction. L_{box} consists of L_1 loss and generalized IoU loss [69] for box regression.

3.2 RelTR Model

As shown in Fig. 2, our one-stage model RelTR has an encoder-decoder architecture, which directly predicts N_t triplets without inferring the possible predicates between all entity pairs. It consists of the feature encoder extracting the visual feature context, the entity decoder capturing the entity representations from DETR [18] and the triplet decoder with the subject and object branches.

A triplet decoder layer contains three attention functions, coupled self-attention (CSA), decoupled visual attention (DVA) and decoupled entity attention (DEA), respectively. Given N_t coupled subject and object queries, the triplet decoder layer reasons about the feature context Z and entity representations Q_e from the entity decoder layer to directly output the information of N_t triplets without inferring the possible predicates between all entity pairs.

3.2.1 Subject and Object Queries.

There are two types of embeddings, namely subject queries $Q_s \in \mathbb{R}^{N_t \times d}$ and object queries $Q_o \in \mathbb{R}^{N_t \times d}$, for the subject branch and object branch respectively. These N_t pairs of subject and object queries are transformed into N_t pairs of subject and object representations of size d. However, the subject query and the object query are not actually linked together in a query pair since the attention layers in the triplet decoder are permutation invariant. In order to distinguish between different triplets, the learnable triplet encodings $E_t \in \mathbb{R}^{N_t \times d}$ are introduced.

3.2.2 Coupled Self-Attention (CSA)

captures the context between N_t triplets, and the dependencies between all subjects and objects. Although the triplet encodings E_t are already available, we still need subject encodings E_s and object encodings E_o of the same size as E_t to inject the semantic concepts of `<subject>` and `<object>` in coupled self-attention. The subject and object embeddings are encoded and the output of CSA can be formulated as:

$$Q = K = [Q_s + E_s + E_t, Q_o + E_o + E_t]$$
$$[Q_s, Q_o] = Att_{CSA}(Q, K, [Q_s, Q_o]), \tag{3}$$

where $[,]$ indicates the unordered concatenation operation and the updated embeddings keep the original symbols unchanged for brevity. The output of CSA $[Q_s, Q_o]$ is decoupled into Q_s and Q_o which continue to be used for the subject branch and the object branch, respectively.

3.2.3 Decoupled Visual Attention (DVA)

concentrates on extracting visual features from the feature context Z. *Decoupled* means that the computations of subject and object embeddings are independent of each other, which is distinct from CSA. In the subject branch, subject embeddings $Q_s \in \mathbb{R}^{N_t \times d}$ are updated through their interaction with the feature context $Z \in \mathbb{R}^{HW \times d}$. The feature context combines with fixed position encodings $E_p \in \mathbb{R}^{HW \times d}$ again in DVA. The updated subject embeddings containing visual features are presented as:

$$Q = Q_s + E_t, K = Z + E_p$$
$$Q_s = Att_{DVA}^{(sub)}(Q, K, Z). \tag{4}$$

The same operation is performed in the object branch. In the multi-head attention operation, N_t attention heat maps $M_s \in \mathbb{R}^{N_t \times HW}$ are computed. We also adopt the reshaped heat maps as a spatial feature for predicate classification.

3.2.4 Decoupled Entity Attention (DEA)

is performed as the bridge between entity detection and triplet detection. Entity representations $Q_e \in \mathbb{R}^{N_e \times d}$ can provide localization and classification information with higher quality due to the fact that they do not have semantic restrictions like those between subject and object embeddings. The motivation for introducing DEA is expecting subject and object embeddings to learn more accurate localization and classification information from entity representations through the attention mechanism. Subject representations Q_s and object representations Q_o are finally updated in a triplet decoder layer as follows:

$$Q_s = Att_{DEA}^{(sub)}(Q_s + E_t, Q_e, Q_e)$$
$$Q_o = Att_{DEA}^{(obj)}(Q_o + E_t, Q_e, Q_e), \tag{5}$$

where $Att_{DEA}^{(sub)}$ and $Att_{DEA}^{(obj)}$ are the decoupled entity attention modules in the subject and object branch. The outputs of DEA are processed by a feed-forward network followed by a normalization layer with residual connection. The feed-forward network (FFN) consist of two linear transformation layers with ReLU activation.
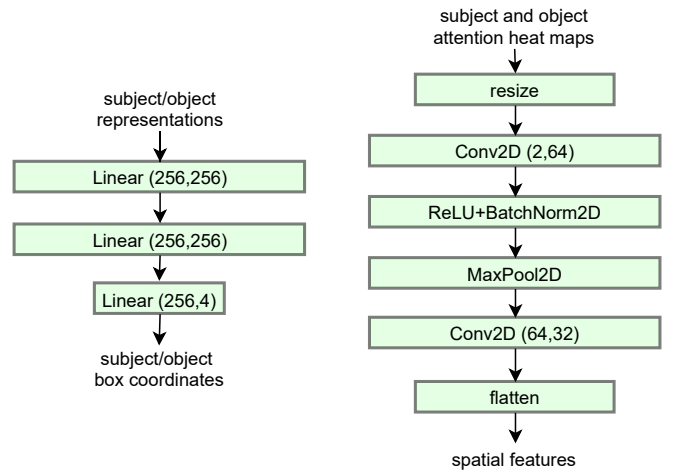

Fig. 3: *Left*: Architecture of the feed-forward network for subject/object box regression. *Right*: Architecture of the convolutional mask head.
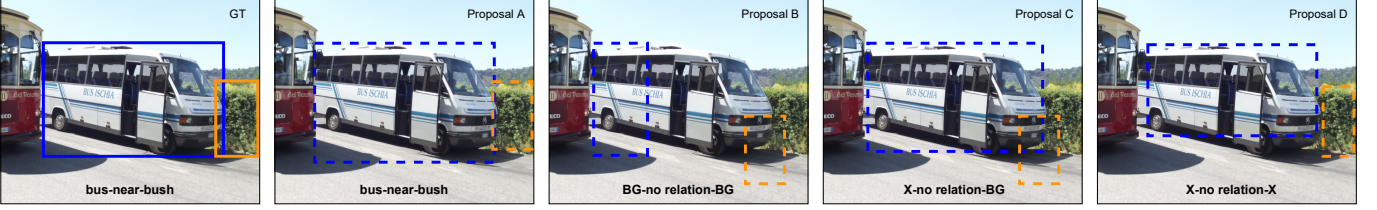
Fig. 4: The ground truth is assigned to Proposal A while `<background-no relation-background>` is assigned to Proposal B. However, `<background>` should not be assigned to the subject of Proposal C and the subject as well as object of Proposal D. **BG** denotes `<background>` while **X** indicates no assignment.

3.2.5 Final Inference.

A complete triplet includes the predicate label and the class labels as well as the bounding box coordinates of the subject and object. The subject representations Q_s and object representations Q_o from the last decoder layer are transformed by two linear projection layers into entity class distributions. We utilize two independent feed-forward networks with the same structure to predict the height, width and normalized center coordinates of subject and object boxes. The architecture is shown in Fig. 3 (left). A pair of subject attention heat map M_s and object attention heatmap M_o from DVA modules in the last decoder layer is concatenated and resized $2 \times 28 \times 28$.. The convolutional mask head shown in Fig. 3 (right) converts the attention heat maps to spatial feature vectors. The final predicate labels are predicted by a two-layer perceptron with the subject representations, object representations and spatial feature vectors.

3.3 Set Prediction Loss for Triplet Detection

We design a set prediction loss for triplet detection by extending the entity detection set prediction loss in Eq. 2. We present a triplet prediction as $\langle \hat{y}_{sub}, \hat{c}_{prd}, \hat{y}_{obj} \rangle$ where $\hat{y}_{sub} = \{\hat{c}_{sub}, \hat{b}_{sub}\}$ and $\hat{y}_{obj} = \{\hat{c}_{obj}, \hat{b}_{obj}\}$ while a ground truth is denoted as $\langle y_{sub}, c_{prd}, y_{obj} \rangle$. The predicted subject, predicate and object labels are respectively denoted as $\hat{c}_{sub}$, $\hat{c}_{prd}$ and $\hat{c}_{obj}$ while the box coordinates of the subject and object are denoted as $\hat{b}_{sub}$ and $\hat{b}_{obj}$.

When N_t relationships are predicted and N_t is larger than the number of triplets in the image, the ground truth set of triplets is padded with Φ `<background-no relation-background>`. The pair-wise matching cost c_{tri} between a predicted triplet and a ground truth triplet consists of the subject cost $c_m(\hat{y}_{sub}, y_{sub})$, object cost $c_m(\hat{y}_{obj}, y_{obj})$ and predicate cost $c_m(\hat{c}_{prd}, c_{prd})$. The prediction $\hat{y} = \{\hat{c}, \hat{b}\}$ contains the predicted class $\hat{c}$ including the class probabilities $\hat{p}$ and the predicted box coordinates $\hat{b}$ while the ground truth $y = \{c, b\}$ contains the ground truth class c and the ground truth box b. For the predicate, we only have the predicted class $\hat{c}_{prd}$ and ground truth class c_{prd}.

The subject/object cost is determined by the predicted entity class probability and the predicted bounding box while the predicate cost is determined only by the predicted predicate class probability. We define the predicted probability of class c as $\hat{p}(c)$. We adopt the class cost function

from [65] which can be formulated as:

$$c_{cls}^+(\hat{c}, c) = \alpha \cdot (1 - \hat{p}(c))^\gamma \cdot (-log(\hat{p}(c) + \varepsilon))$$
$$c_{cls}^-(\hat{c}, c) = (1 - \alpha) \cdot \hat{p}(c)^\gamma \cdot (-log(1 - \hat{p}(c) + \varepsilon)) \quad (6)$$
$$c_{cls}(\hat{c}, c) = c_{cls}^+(\hat{c}, c) - c_{cls}^-(\hat{c}, c),$$

where α, γ and ε are respectively set to 0.25, 2 and 10^{-8}. The box cost for the subject and object is computed using L_1 loss and generalized IoU loss [69]:

$$c_{box}(\hat{b}, b) = 5L_1(\hat{b}, b) + 2L_{GIoU}(\hat{b}, b). \quad (7)$$

The cost function c_m can be presented as:

$$c_m(\hat{y}, y) = c_{cls}(\hat{c}, c) + \mathbb{1}_{\{b \in y\}} c_{box}(\hat{b}, b), \quad (8)$$

where $b \in y$ denotes that the ground truth includes the box coordinates (only for the subject/object cost). The cost between a triplet prediction and a ground truth triplet is computed as:

$$c_{tri} = c_m(\hat{y}_{sub}, y_{sub}) + c_m(\hat{y}_{obj}, y_{obj}) + c_m(\hat{c}_{prd}, c_{prd}), \quad (9)$$

Given the triplet cost matrix C_{tri}, the Hungarian algorithm is executed for the bipartite matching and each ground truth triplet is assigned to a prediction. However, `<background-no relation-background>` should not be assigned to all predictions that do not match the ground truth triplets. After several iterations of training, RelTR is likely to output the triplet proposals in four possible ways, as demonstrated in Fig. 4. Assigning ground truth to Proposal A and `<background-no relation-background>` to Proposal B are two clear cases. For Proposal C, `<background>` should not be assigned to the subject due to the poor object prediction. Furthermore, `<background>` should not be assigned to the subject and object of Proposal D due to the fact that there is a better candidate Prediction A. To solve this problem, we integrate an IoU-based assignment strategy in our set prediction loss: For a triplet prediction, if the predicted subject or object label is correct, and the IoU of the predicted box and ground truth box is greater than or equal to the threshold T, the loss function does not compute a loss for the subject or object. The set prediction loss for triplet detection is formulated as:

$$L_{sub} = \sum_{i=1}^{N_t} \Theta \left[L_{cls} + \mathbb{1}_{\{c_{sub}^i \neq \phi\}} L_{box} \right]$$

$$L_{obj} = \sum_{i=1}^{N_t} \Theta \left[L_{cls} + \mathbb{1}_{\{c_{obj}^i \neq \phi\}} L_{box} \right] \quad (10)$$

$$L_{triplet} = L_{sub} + L_{obj} + L_{cls}^{prd},$$

	Method	AP_{50}	PredCLS				SGCLS				SGDET				#params(M)	FPS
			R@20	R@50	mR@20	mR@50	R@20	R@50	mR@20	mR@50	R@20	R@50	mR@20	mR@50		
two-stage	MOTIFS [9]	20.0	58.5	65.2	10.8	14.0	32.9	35.8	6.3	7.7	21.4	27.2	4.2	5.7	240.7	6.6
	KERN [10]	20.0	59.1	65.8	-	17.7	32.2	36.7	-	9.4	22.3	27.1	-	6.4	405.2	4.6
	RelDN [56]	-	66.9	68.4	-	-	36.1	36.8	-	-	21.1	28.3	-	-	615.6	4.7
	VCTree-TDE [59]	28.1	39.1	49.9	17.2	23.3	22.8	28.8	8.9	11.8	14.3	19.6	6.3	9.3	360.8	1.2
	GPS-Net [48]	-	**67.6**	**69.7**	**17.4**	21.3	**41.8**	**42.3**	**10.0**	11.8	22.3	28.9	6.9	8.7	-	-
	BGNN [46]	29.0	-	59.2	-	**30.4**	-	37.4	-	**14.3**	**23.3**	**31.0**	**7.5**	**10.7**	341.9	2.3
	IMP [42]	-	58.5	65.2	-	9.8	31.7	34.6	-	5.8	14.6	20.7	-	3.8	**203.8**	**10.0**
	CISC [33]	-	42.1	53.2	-	-	23.3	27.8	-	-	7.7	11.4	-	-	-	-
	G-RCNN [44]	24.8	-	54.2	-	-	-	29.6	-	-	-	11.4	-	-	-	-
one-stage	FCSGG [60]	28.5	33.4	41.0	4.9	6.3	19.0	23.5	2.9	3.7	16.1	21.3	2.7	3.6	87.1	8.3*
	RelTR (ours)	26.4	*63.1*	*64.2*	*20.0*	*21.2*	*29.0*	*36.6*	*7.7*	*11.4*	*20.2*	*25.2*	*5.8*	*8.5*	*63.7*	*16.6*

TABLE 1: Comparison with state-of-the-art scene graph generation methods on Visual Genome [19] test set. These methods are divide into two-stage and one-stage. The best numbers in two-stage methods are shown in **bold**, and the best numbers in one-stage methods are shown in *italic*. Models that use prior knowledge are represented in blue, to distinguish them from visual-based models. The inference speed (FPS) of different models is tested on the same RTX 2080Ti of batch size 1. Note that the number of FCSGG is directly taken from [60] due to unavailable code.

where L_{cls}^{prd} is the cross-entropy loss for predicate classification. Θ is 0, when `<background>` is assigned to the subject/object but the label is predicted correctly and the box overlaps with the ground truth IoU$\geqslant T$; in other cases, Θ is 1. The total loss function is computed as:

$$L_{total} = L_{entity} + L_{triplet}. \tag{11}$$

4 EXPERIMENTS

4.1 Datasets and Evaluation Settings

4.1.1 Visual Genome

We followed the widely used Visual Genome [19] split proposed by [42]. There are a total of 108k images in the dataset with 150 entity categories and 50 predicate categories. 70% of the images are divided into the training dataset and the remaining 30% are used as the test set. 5k images are further drawn from the training set for validation. There are three standard evaluation settings: (1) Predicate classification (**PredCLS**): predict predicates given ground truth categories and bounding boxes of entities. (2) Scene graph classification (**SGCLS**): predict predicates and entity categories given ground truth boxes. (3) Scene graph detection (**SGDET**): predict categories, bounding boxes of entities and predicates. Distinct from two-stage methods, the ground truth bounding boxes and categories of entities cannot be given directly. Therefore, we assign the ground truth information to the matched triplet proposals when evaluating RelTR on **PredCLS**/**SGCLS**. Recall@k (R@k), mean Recall@k (mR@k) are adopted to evaluate the algorithm performance [2], [37].

4.1.2 Open Images V6

We also conduct experiments on the large-scale Open Images V6 [20] consisting of 126k training images, 5.3k test images and 1.8k validation images. It involves 288 entity categories and 30 predicate categories. We adopt the standard evaluation metrics used in the Open Images Challenge. Recall@50, weighted mean average precision (AP) of relationship detection wmAP$_{rel}$, and phrase detection wmAP$_{phr}$ are calculated. The final score is computed as: score$_{wtd}$ = 0.2*R@50+0.4*wmAP$_{rel}$ +0.4*wmAP$_{phr}$.

4.2 Implementation Details

We adopt the same hyperparameters in our experiments on Visual Genome and Open Images. We train RelTR for 150 epochs on 8 RTX 2080 Ti GPUs with AdamW [70] setting the batch size to 2 per GPU, weight decay to 10^{-4} and clipping the gradient norm> 0.1. The initial learning rates of the Transformer and ResNet-50 backbone are set to 10^{-4} and 10^{-5} respectively and the learning rates are dropped by 0.1 after 100 epochs. In the training we also use auxiliary losses [71] for the triplet decoder as [18], [65] did. By default, RelTR has 6 encoder layers and 6 triplet decoder layers. The number of triplet decoder layers and the number of entity decoder layers are set to be the same. The multi-head attention modules with 8 heads in our model are trained with dropout of 0.1. For all experiments, the model dimension d is set to 256. If not specifically stated, the number of entity queries N_e and coupled queries N_t are respectively set to 100 and 200 while the IoU threshold in the triplet assignment is 0.7. For fair comparison, inference speeds (FPS) of all the reported SGG models are evaluated on a single RTX 2080 Ti with the same hardware configuration. For computing the inference speed (FPS), we average over all the test images, where for each image, the time cost for start timing when an image is given as input and end timing when triplet proposals are output as the inference time. The time cost for evaluating the whole dataset is not included.

4.3 Quantitative Results and Comparison

4.3.1 Visual Genome

We compare scores of R@K and mR@K, number of parameters and inference speed on SGDET (FPS) with several two-stage models and one-stage model FCSGG [60] in Table 1. Models that not only use visual appearance, but also prior knowledge (e.g. semantic and statistic information) are represented in blue, to distinguish them from visual-based models. Overall, the two-stage models have higher scores of R@K and mR@K than the one-stage models while they have more parameters and slower inference speed. This phenomenon also occurs between the models using prior information and visual-based models. Noted that the performance of the entity detectors in the two-stage models has a significant impact on the model's scores, especially on SGDET. Our model achieves R@50 = 25.2 and mR@50 = 8.5 on SGDET, which is respectively 3.9 and 4.9 points higher
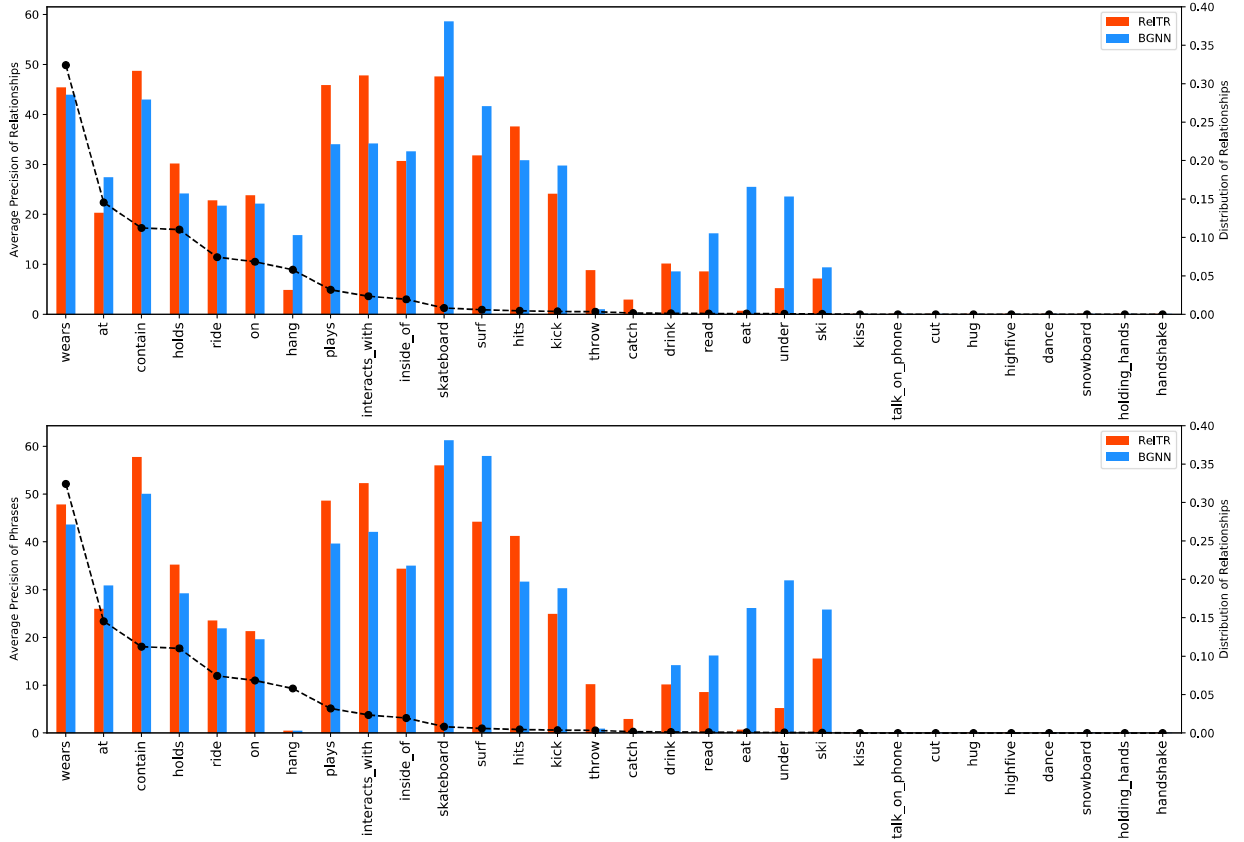
Fig. 5: Average precision of relationships and phrases for RelTR and BGNN on Open Images V6. The distribution of relationships in the test set is shown with the black dash line. The average precision of relationships of RelTR is higher than BGNN for 7 of the top-10 high frequency predicates while BGNN generally performs better than RelTR for the low frequency predicates (`skateboard` to `ski`). We conjecture that it is attributed to prior knowledge used in BGNN. The overall trend of AP_{phr} is the same as AP_{rel} except `hang`.

than another one-stage model FCSGG [60]. Our model is also competitive compared with recent two-stage models, and outperforms state-of-the-art visual-based methods. Although the R@20/R@50 score of RelTR is 3.1/5.8 points lower than that of BGNN [46], RelTR is a light-weight model, which has only 63.7M parameters and an inference speed of 16.6 FPS, ca. 7 times faster than BGNN. This allows RelTR to be used in a wide range of practical applications. For PredCLS and SGCLS, the ground truth bounding boxes and labels of entities cannot be given to RelTR directly. Therefore, we replace the predicted boxes and labels of the matched triplet proposals by the ground truth information and RelTR achieves R@50 = 64.2 and mR@50 = 21.2 on PredCLS while R@50 = 36.6 and mR@50 = 11.4 on SGCLS.

4.3.2 Open Images V6

We train RelTR on the Open Images V6 dataset and compare with other two-stage methods, as shown in Table 2. Although R@50 of RelTR is 10.87 points lower than the best two-stage method VCTree [37], RelTR has the highest $wmAP_{rel}$ (0.66 points higher than BGNN [46]) and $wmAP_{phr}$ (3.13 points higher than VCTree [37]). The final weighted score of RelTR is only 0.43 points lower than the best two-stage model, which is a very small performance gap. The inference speed of RelTR is 16.9 FPS, ca. 6 and 9 times faster than BGNN and VCTree, respectively.

Method	R@50	$wmAP_{rel}$	$wmAP_{phr}$	$score_{wtd}$	FPS
RelDN [56]	73.08	32.16	33.39	40.84	5.3
VCTree [37]	**75.34**	33.21	34.31	**41.97**	1.9
G-RCNN [44]	74.51	33.15	34.21	41.84	-
Motifs [9]	71.63	29.91	31.59	38.93	7.4
GPS-NET [48]	74.81	32.85	33.98	41.69	-
BGNN [46]	74.98	33.51	34.15	41.69	2.9
RelTR (ours)	64.47	**34.17**	**37.44**	41.54	**16.9**

TABLE 2: Comparison with other two-stage methods on the Open Images V6 [20] test set. The numbers of these state-of-the-art methods are taken from [46].

To further demonstrate the performance of RelTR, we compare the average precision (AP) of relationships and phrases for RelTR and BGNN [46] (see Fig. 5) with Open Images V6. Although the R@50 of RelTR is lower, RelTR outperforms BGNN on the weighted mean AP of relationships and phrases. The distribution of relationships in the Open Images V6 test set is also shown with the black dash lines. There are 9 predicates (`kiss` to `handshake`) that do not appear in the test set. The average precision of relationships AP_{rel} and AP_{phr} of RelTR are higher than BGNN for 7 of the top-10 high frequency predicates. For the low frequency predicates (`skateboard` to `ski`), BGNN generally performs better than RelTR. We conjecture that it is attributed to prior knowledge used in BGNN.

4.4 Ablation Studies

In the ablation studies, we consider how the following aspects influence the final performance. All the ablation studies are performed with Visual Genome dataset [19].

4.4.1 Number of Layers.

The feature encoder layer and triplet decoder layer have different effects on the performance, size and inference speed. When the number of encoder layers varies, we keep the number of triplet decoder layers always 6, and vice versa. When there is no encoder layer, the decoder reasons about the feature map without context and R@50 drops by 4.1 points significantly (see Table 3). Adding an encoder layer brings fewer parameters compared to adding a triplet decoder layer. Because the decoder is indispensable for scene graph generation, the minimum number of triplet decoder layers in our experiment is set to 3. When the number of triplet decoder layers is increased to 6, the improvement of R@20, R@50 and R@100 are obvious. In contrast, there is a small decrease in performance when the number of triplet decoder layers is increased to 9. We conjecture that this may be caused by overfitting.

Layer Number		SGDET			#params(M)	FPS
Encoder	Triplet Decoder	R@20	R@50	R@100		
0	6	16.6	21.1	23.8	**55.8**	**18.7**
3	6	19.7	24.4	26.5	59.7	17.7
9	6	**20.6**	**25.3**	**27.6**	67.6	16.0
6	6	20.2	25.2	27.5	63.7	16.6
6	3	18.4	23.4	26.4	48.7	20.4
6	9	20.2	24.9	27.1	78.7	14.2

TABLE 3: Impact of the number of encoder and decoder layers on the performance, model size and inference speed.

4.4.2 Module Effectiveness.

We only ablate Decoupled Entity Attention (DEA) and the mask head for the attention heat maps from the framework since the other modules are essential. Table 4 demonstrates that DEA modules help the model to predict higher quality subjects and objects, and increase R@50 by 0.6 (with the mask head). In comparison, the improvement offered by the mask head is very limited. We hypothesize that the spatial features are already implicit encoded in the visual features generated by DVA modules.

Ablation Setting		SGDET			#params(M)	FPS
DEA	Mask head	R@20	R@50	R@100		
✗	✗	19.7	24.5	26.7	**59.3**	**18.4**
✗	✓	19.8	24.6	26.9	60.5	17.9
✓	✗	20.1	25.0	27.1	62.5	17.3
✓	✓	**20.2**	**25.2**	**27.4**	63.7	16.6

TABLE 4: Decoupled entity attention (DEA) and the mask head for the attention heat maps are isolated separately from the framework. ✗ denotes the module is ablated.

4.4.3 Threshold in Set Prediction Loss

The IoU threshold T of the IoU-based assignment strategy in the set prediction loss for triplet detection is varied from 0.6 to 1. Since a prediction box overlaps with the ground truth box of IoU= 1 is almost impossible in practice, the

strategy can be considered as deactivated when $T = 1$. Two curves, namely T-R@50 and T-mR@50 on SGDET, are shown in Fig. 6. When our assignment strategy is deactivated ($T = 1$), the model performs the worst. As T increases from 0.7 to 1, the overall trend of the two curves is decreasing. This is more evident for the T-mR@50 curve.
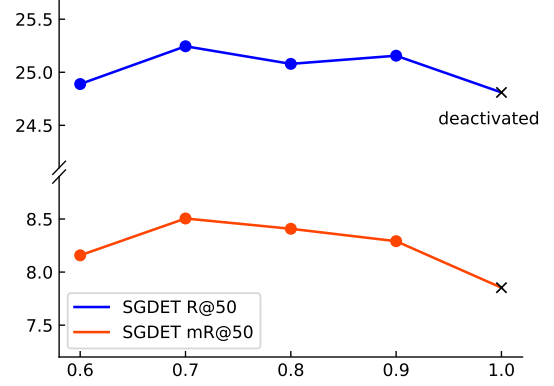

Fig. 6: T-R@50 and T-mR@50 curve on SGDET. × indicates that the IoU-based assignment strategy is deactivated.
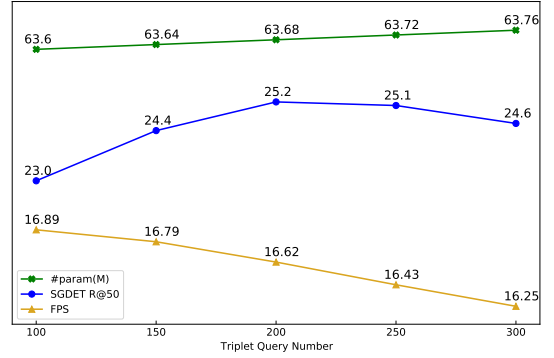

Fig. 7: Changes in the parameter number, performance and FPS as the triplet number N_t varies.

4.5 Analysis on Subject and Object Queries

Distinct from the two-stage methods which output N object proposals after NMS and then label $N(N − 1)$ predicates, RelTR predicts N_t triples directly by N_t subject and object queries interacting with an image. We trained the model on Visual Genome using different N_t. Fig. 7 shows that as the number of coupled subject and object queries increases linearly, the parameters of the model increase linearly whereas the inference speed decreases linearly. However, the performance varies non-linearly and the best performance is achieved when $N_t = 200$ for the Visual Genome dataset. Too many queries generate many incorrect triplet proposals that take the place of correct proposals in the recall list.

To explore how RelTR infers triplets with the coupled subject and object queries, we collect predictions from a random sample of 5000 images from Visual Genome test set. We visualize the predictions for 10 out of total 200 coupled queries. Fig. 8 shows the spatial and class distributions of subjects and objects, as well as the class distribution of top-5 predicates in the 5000 predictions of 10 coupled subject
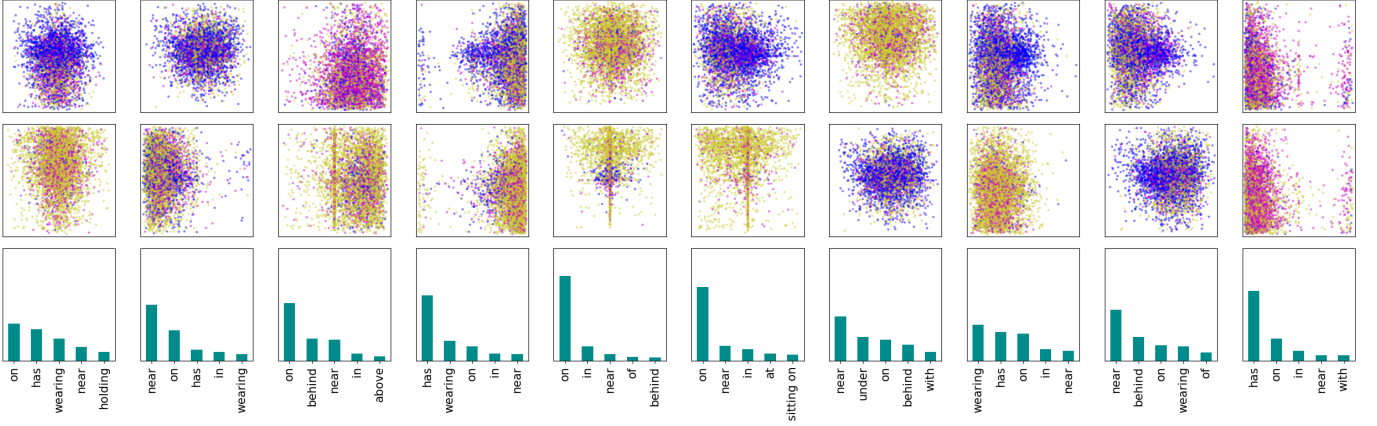
Fig. 8: Predictions on 5000 images from Visual Genome test set are presented for 10 coupled subject and object queries. The size of all images is normalized to 1×1, with each point in the first and second rows representing the box center of a subject and an object in a prediction respectively. Different point colors denote different entity super-categories: (1) blue for humans (child, person and woman etc.) (2) plum for things that exist in nature (beach, dog and head etc.) (3) yellow for man-made objects (cup, jacket and table etc.). The corresponding distributions of top-5 predicate are shown in the third row.

and object queries. It demonstrates that different coupled queries learn different patterns from the training data, and attend to different classes of triplets in different regions at the inference.

4.6 Qualitative Results

Fig. 9 shows the qualitative results for scene graph generation (SGDET) of Visual Genome dataset. Although some other proposals are also meaningful, we only demonstrate 9 relationships with the highest confidence scores and the generated scene graph due to space limitations in Fig. 9. Blue boxes are the subject boxes while orange boxes are the object boxes. Attention scores are displayed in the same color as boxes. The overlap of subject and object attention is shown in white. The ground truth annotations of the two images are demonstrated in Fig. 10. For brevity, we only show the bounding boxes of the entities that appear in the annotated triplets.

For the first image (with the car and building), we can assume that the 9 output triplets are all correct. The prediction `<car-in front of-building>` indicates that RelTR can understand spatial relationships from 2D image to some extent (`in front of` is not a high-frequent predicate in Visual Genome). However, R@9 of the first image is only 5/12 = 41.7 because of the preferences in the ground truth triplet annotations. This phenomenon is more evident in the second image (with the woman and computer). Note that in the used Visual Genome-150 split [42] there is no `computer` class but only `laptop` class. 6 out of 9 predictions from RelTR can be considered valid whereas R@9 is 0 due to the labeling preference. Sometimes RelTR outputs some duplicate triplets such as `<woman-wearing-jean>` and `<woman-looking at-laptop>` in the second image. Along with the output results, RelTR also shows the regions of interest for the output relationships, making the behavior of the model easier to interpret.

The qualitative results of SGDET for Open Images V6 are shown in Fig. 11. Different from the dense triplets in

the annotations of VG, each image from Open Images V6 is labeled with 2.8 triplets on average. Therefore, we only show the most confident triplet from predictions for each image.

5 CONCLUSION

In this paper, based on Transformer's encoder-decoder architecture, we propose a novel one-stage end-to-end framework for scene graph generation, RelTR. Given a fixed number of coupled subject and object queries, a fixed-size set of relationships is predicted using different attention mechanisms in the triplet decoder of RelTR. An IoU-based assignment strategy is proposed to optimize the triplet prediction-ground truth assignment during the model training. Compared with other state-of-the-art methods, RelTR achieves competitive performance using only visual appearance, with very few model parameters and fast inference.

REFERENCES

[1] J. Johnson, R. Krishna, M. Stark, L.-J. Li, D. Shamma, M. Bernstein, and L. Fei-Fei, "Image retrieval using scene graphs," in *Proceedings of the IEEE conference on computer vision and pattern recognition*, 2015, pp. 3668–3678. 1, 2

[2] C. Lu, R. Krishna, M. Bernstein, and L. Fei-Fei, "Visual relationship detection with language priors," in *European conference on computer vision*. Springer, 2016, pp. 852–869. 1, 2, 6

[3] K. Nguyen, S. Tripathi, B. Du, T. Guha, and T. Q. Nguyen, "In defense of scene graphs for image captioning," in *Proceedings of the IEEE/CVF International Conference on Computer Vision (ICCV)*, 2021, pp. 1407–1416. 1

[4] L. Gao, B. Wang, and W. Wang, "Image captioning with scene-graph based semantic concepts," in *Proceedings of the 2018 10th International Conference on Machine Learning and Computing*, 2018, pp. 225–229. 1

[5] J. Johnson, B. Hariharan, L. Van Der Maaten, J. Hoffman, L. Fei-Fei, C. Lawrence Zitnick, and R. Girshick, "Inferring and executing programs for visual reasoning," in *Proceedings of the IEEE International Conference on Computer Vision*, 2017, pp. 2989–2998. 1

[6] O. Ashual and L. Wolf, "Specifying object attributes and relations in interactive scene generation," in *Proceedings of the IEEE/CVF International Conference on Computer Vision*, 2019, pp. 4561–4569. 1

Fig. 9: Qualitative results for scene graph generation of Visual Genome dataset. The top-9 relationships with confidence and the generated scene graph are shown. Boxes and attention scores of subjects are colored with blue while objects with orange. The orange vertices in the generated scene graph indicate the predictions are duplicated. The computer is classified as laptop in the second image since there is no computer class but only laptop class in the used VG-150 split [42]. Compared with the ground truth annotations in Fig. 10, the predictions of RelTR are diverse. Although sometimes RelTR cannot label very difficult relationships correctly (e.g. looking at), the results demonstrate that the generated scene graphs are of high quality.

[7] J. Johnson, A. Gupta, and L. Fei-Fei, "Image generation from scene graphs," in *Proceedings of the IEEE conference on computer vision and pattern recognition*, 2018, pp. 1219–1228. 1

[8] S. Ren, K. He, R. Girshick, and J. Sun, "Faster r-cnn: towards real-time object detection with region proposal networks," *IEEE transactions on pattern analysis and machine intelligence*, vol. 39, no. 6, pp. 1137–1149, 2016. 1

[9] R. Zellers, M. Yatskar, S. Thomson, and Y. Choi, "Neural motifs: Scene graph parsing with global context," in *Proceedings of the IEEE Conference on Computer Vision and Pattern Recognition*, 2018, pp. 5831–5840. 1, 2, 6, 7

[10] T. Chen, W. Yu, R. Chen, and L. Lin, "Knowledge-embedded routing network for scene graph generation," in *Proceedings of the IEEE/CVF Conference on Computer Vision and Pattern Recognition*, 2019, pp. 6163–6171. 1, 6

[11] R. Yu, A. Li, V. I. Morariu, and L. S. Davis, "Visual relationship detection with internal and external linguistic knowledge distillation," in *Proceedings of the IEEE international conference on computer vision*, 2017, pp. 1974–1982. 1, 2

[12] A. Zareian, S. Karaman, and S.-F. Chang, "Bridging knowledge graphs to generate scene graphs," in *European Conference on Computer Vision*, 2020, pp. 606–623. 1

[13] J. Gu, H. Zhao, Z. Lin, S. Li, J. Cai, and M. Ling, "Scene graph generation with external knowledge and image reconstruction," in *Proceedings of the IEEE/CVF Conference on Computer Vision and Pattern Recognition*, 2019, pp. 1969–1978. 1

[14] H. Law and J. Deng, "Cornernet: Detecting objects as paired keypoints," in *Proceedings of the European conference on computer*

window4-on-building0
window2-on-building0
window5-on-building0
door3-on-building0
window7-on-building0
wheel10-on-car1
wheel10-on-car1
window9-on-car1
window8-on-car1
tire6-on-car1
tire6-on-car1
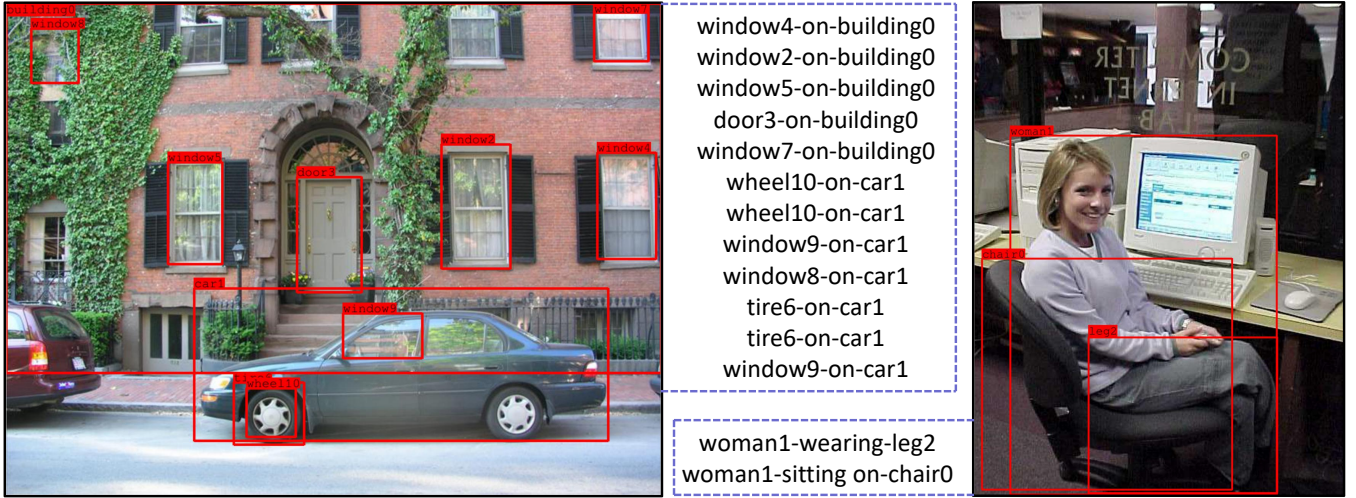window9-on-car1

woman1-wearing-leg2
woman1-sitting on-chair0

Fig. 10: Ground truth annotations of the two images in Fig. 9 from Visual Genome dataset. For brevity, only the bounding boxes of the entities that appears in the annotated triplets are shown with red. All entities are numbered to distinguish between entities of the same class. There are two errors in the ground truth annotations: `<window8-on-car1>` in the first image and `<woman1-wearing-leg2>` in the second image. There could be duplicate triplets in the ground truth (e.g. `<wheel10-on-car1>` in the first image). For the first image, only the relationships with the predicate `on` are labeled while for the second image, the relationships such as `<woman1-wearing-shirt>` are omitted. These biases in the ground truth annotations lead to the low score of R@K, the other SGG models also suffer from this problem.

Girl-holds-Guitar   Flowerpot-contain-Houseplant   Woman-wears-Glasses   Man-hits-Football   Chair-at-Coffee table

Fig. 11: Qualitative results for scene graph generation of Open Images V6. Different from the dense triplets in the annotations of VG, each image from Open Images V6 is labeled with 2.8 triplets on average. Although Open Images V6 contains more entity classes, the image scenarios are simpler compared to Visual Genome. Therefore, only the top-1 triplets are shown in the second row while the original images are in the first row. Boxes and attention scores of subjects are also colored with blue while objects with orange. RelTR demonstrates the excellent quality of its confident triplet proposals.

vision (ECCV), 2018, pp. 734–750. 1

[15] Z. Tian, C. Shen, H. Chen, and T. He, "Fcos: Fully convolutional one-stage object detection," in *Proceedings of the IEEE/CVF international conference on computer vision*, 2019, pp. 9627–9636. 1

[16] X. Zhou, D. Wang, and P. Krähenbühl, "Objects as points," *arXiv preprint arXiv:1904.07850*, 2019. 1

[17] P. Sun, Y. Jiang, E. Xie, W. Shao, Z. Yuan, C. Wang, and P. Luo, "What makes for end-to-end object detection?" in *International Conference on Machine Learning*. PMLR, 2021, pp. 9934–9944. 1

[18] N. Carion, F. Massa, G. Synnaeve, N. Usunier, A. Kirillov, and S. Zagoruyko, "End-to-end object detection with transformers," in *European Conference on Computer Vision*. Springer, 2020, pp. 213–229. 1, 2, 3, 4, 6

[19] R. Krishna, Y. Zhu, O. Groth, J. Johnson, K. Hata, J. Kravitz, S. Chen, Y. Kalantidis, L.-J. Li, D. A. Shamma *et al.*, "Visual genome: Connecting language and vision using crowdsourced dense image annotations," *International journal of computer vision*, vol. 123, no. 1, pp. 32–73, 2017. 2, 3, 6, 8

[20] A. Kuznetsova, H. Rom, N. Alldrin, J. Uijlings, I. Krasin, J. Pont-Tuset, S. Kamali, S. Popov, M. Malloci, A. Kolesnikov *et al.*, "The open images dataset v4," *International Journal of Computer Vision*, vol. 128, no. 7, pp. 1956–1981, 2020. 2, 3, 6, 7

[21] X. Yang, K. Tang, H. Zhang, and J. Cai, "Auto-encoding scene graphs for image captioning," in *Proceedings of the IEEE/CVF Conference on Computer Vision and Pattern Recognition*, 2019, pp. 10 685–10 694. 2

[22] J. Gu, S. Joty, J. Cai, H. Zhao, X. Yang, and G. Wang, "Unpaired image captioning via scene graph alignments," in *Proceedings of the IEEE/CVF International Conference on Computer Vision*, 2019, pp. 10 323–10 332. 2

[23] K.-H. Lee, H. Palangi, X. Chen, H. Hu, and J. Gao, "Learning visual relation priors for image-text matching and image captioning with neural scene graph generators," *arXiv preprint arXiv:1909.09953*, 2019. 2

[24] J. Shi, H. Zhang, and J. Li, "Explainable and explicit visual reasoning over scene graphs," in *Proceedings of the IEEE/CVF Conference on Computer Vision and Pattern Recognition (CVPR)*, 2019. 2

[25] ——, "Explainable and explicit visual reasoning over scene graphs," in *Proceedings of the IEEE/CVF Conference on Computer Vision and Pattern Recognition*, 2019, pp. 8376–8384. 2

[26] S. Lee, J.-W. Kim, Y. Oh, and J. H. Jeon, "Visual question answering over scene graph," in *International Conference on Graph Computing (GC)*, 2019, pp. 45–50. 2

[27] Y. Li, T. Ma, Y. Bai, N. Duan, S. Wei, and X. Wang, "Pastegan: A semi-parametric method to generate image from scene graph," *Advances in Neural Information Processing Systems*, vol. 32, pp. 3948–3958, 2019. 2

[28] A. Talavera, D. S. Tan, A. Azcarraga, and K.-L. Hua, "Layout and context understanding for image synthesis with scene graphs," in *IEEE International Conference on Image Processing (ICIP)*, 2019, pp. 1905–1909. 2

[29] S. Tripathi, A. Bhiwandiwalla, A. Bastidas, and H. Tang, "Using scene graph context to improve image generation," *arXiv preprint arXiv:1901.03762*, 2019. 2

[30] C. Galleguillos, A. Rabinovich, and S. Belongie, "Object categorization using co-occurrence, location and appearance," in *2008 IEEE Conference on Computer Vision and Pattern Recognition*. IEEE, 2008, pp. 1–8. 2

[31] S. Gould, J. Rodgers, D. Cohen, G. Elidan, and D. Koller, "Multiclass segmentation with relative location prior," *International journal of computer vision*, vol. 80, no. 3, pp. 300–316, 2008. 2

[32] Y. Cong, H. Ackermann, W. Liao, M. Y. Yang, and B. Rosenhahn, "Nodis: Neural ordinary differential scene understanding," in *Proceedings of the European Conference on Computer Vision (ECCV)*, 2020, pp. 636–653. 2

[33] W. Wang, R. Wang, S. Shan, and X. Chen, "Exploring context and visual pattern of relationship for scene graph generation," in *Proceedings of the IEEE/CVF Conference on Computer Vision and Pattern Recognition*, 2019, pp. 8188–8197. 2, 6

[34] J. Shi, Y. Zhong, N. Xu, Y. Li, and C. Xu, "A simple baseline for weakly-supervised scene graph generation," in *Proceedings of the IEEE/CVF International Conference on Computer Vision*, 2021, pp. 16 393–16 402. 2

[35] W. Wang, R. Wang, and X. Chen, "Topic scene graph generation by attention distillation from caption," in *Proceedings of the IEEE/CVF International Conference on Computer Vision*, 2021, pp. 15 900–15 910. 2

[36] Y. Lu, H. Rai, J. Chang, B. Knyazev, G. Yu, S. Shekhar, G. W. Taylor, and M. Volkovs, "Context-aware scene graph generation with seq2seq transformers," in *Proceedings of the IEEE/CVF International Conference on Computer Vision*, 2021, pp. 15 931–15 941. 2

[37] K. Tang, H. Zhang, B. Wu, W. Luo, and W. Liu, "Learning to compose dynamic tree structures for visual contexts," in *Proceedings of the IEEE/CVF Conference on Computer Vision and Pattern Recognition*, 2019, pp. 6619–6628. 2, 6, 7

[38] J. Ji, R. Krishna, L. Fei-Fei, and J. C. Niebles, "Action genome: Actions as compositions of spatio-temporal scene graphs," in *Proceedings of the IEEE/CVF Conference on Computer Vision and Pattern Recognition*, 2020, pp. 10 236–10 247. 2

[39] Y. Cong, W. Liao, H. Ackermann, B. Rosenhahn, and M. Y. Yang, "Spatial-temporal transformer for dynamic scene graph generation," in *Proceedings of the IEEE/CVF International Conference on Computer Vision*, 2021, pp. 16 372–16 382. 2

[40] Y. Teng, L. Wang, Z. Li, and G. Wu, "Target adaptive context aggregation for video scene graph generation," in *Proceedings of the IEEE/CVF International Conference on Computer Vision*, 2021, pp. 13 688–13 697. 2

[41] Y. Lu, C. Chang, H. Rai, G. Yu, and M. Volkovs, "Multi-view scene graph generation in videos," in *International Challenge on Activity Recognition (ActivityNet) CVPR 2021 Workshop*, vol. 3, 2021. 2

[42] D. Xu, Y. Zhu, C. B. Choy, and L. Fei-Fei, "Scene graph generation by iterative message passing," in *Proceedings of the IEEE conference on computer vision and pattern recognition*, 2017, pp. 5410–5419. 2, 6, 9, 10

[43] Y. Li, W. Ouyang, B. Zhou, K. Wang, and X. Wang, "Scene graph generation from objects, phrases and region captions," in *Proceedings of the IEEE international conference on computer vision*, 2017, pp. 1261–1270. 2

[44] J. Yang, J. Lu, S. Lee, D. Batra, and D. Parikh, "Graph r-cnn for scene graph generation," in *Proceedings of the European conference on computer vision (ECCV)*, 2018, pp. 670–685. 2, 6, 7

[45] Y. Li, W. Ouyang, B. Zhou, J. Shi, C. Zhang, and X. Wang, "Factorizable net: an efficient subgraph-based framework for scene graph generation," in *Proceedings of the European Conference on Computer Vision (ECCV)*, 2018, pp. 335–351. 2

[46] R. Li, S. Zhang, B. Wan, and X. He, "Bipartite graph network with adaptive message passing for unbiased scene graph generation," in *Proceedings of the IEEE/CVF Conference on Computer Vision and Pattern Recognition*, 2021, pp. 11 109–11 119. 2, 6, 7

[47] T. Chen, W. Yu, R. Chen, and L. Lin, "Knowledge-embedded routing network for scene graph generation," in *Proceedings of the IEEE/CVF Conference on Computer Vision and Pattern Recognition (CVPR)*, 2019. 2

[48] X. Lin, C. Ding, J. Zeng, and D. Tao, "Gps-net: Graph property sensing network for scene graph generation," in *Proceedings of the IEEE/CVF Conference on Computer Vision and Pattern Recognition*, 2020, pp. 3746–3753. 2, 6, 7

[49] R. Herzig, M. Raboh, G. Chechik, J. Berant, and A. Globerson, "Mapping images to scene graphs with permutation-invariant structured prediction," *Advances in Neural Information Processing Systems*, vol. 31, pp. 7211–7221, 2018. 2

[50] M. Qi, W. Li, Z. Yang, Y. Wang, and J. Luo, "Attentive relational networks for mapping images to scene graphs," in *Proceedings of the IEEE/CVF Conference on Computer Vision and Pattern Recognition*, 2019, pp. 3957–3966. 2

[51] A. Vaswani, N. Shazeer, N. Parmar, J. Uszkoreit, L. Jones, A. N. Gomez, Ł. Kaiser, and I. Polosukhin, "Attention is all you need," in *Advances in neural information processing systems*, 2017, pp. 5998–6008. 2, 3

[52] N. Dhingra, F. Ritter, and A. Kunz, "Bgt-net: Bidirectional gru transformer network for scene graph generation," in *Proceedings of the IEEE/CVF Conference on Computer Vision and Pattern Recognition*, 2021, pp. 2150–2159. 2

[53] R. Koner, P. Sinhamahapatra, and V. Tresp, "Relation transformer network," *arXiv preprint arXiv:2004.06193*, 2020. 2

[54] N. Gkanatsios, V. Pitsikalis, P. Koutras, and P. Maragos, "Attention-translation-relation network for scalable scene graph generation," in *Proceedings of the IEEE/CVF International Conference on Computer Vision Workshops*, 2019, pp. 0–0. 2

[55] Z. Cui, C. Xu, W. Zheng, and J. Yang, "Context-dependent diffusion network for visual relationship detection," in *Proceedings of the 26th ACM international conference on Multimedia*, 2018, pp. 1475–1482. 2

[56] J. Zhang, K. J. Shih, A. Elgammal, A. Tao, and B. Catanzaro, "Graphical contrastive losses for scene graph parsing," in *Proceedings of the IEEE/CVF Conference on Computer Vision and Pattern Recognition*, 2019, pp. 11 535–11 543. 2, 6, 7

[57] B. Dai, Y. Zhang, and D. Lin, "Detecting visual relationships with deep relational networks," in *Proceedings of the IEEE conference on computer vision and Pattern recognition*, 2017, pp. 3076–3086. 2

[58] M. Suhail, A. Mittal, B. Siddiquie, C. Broaddus, J. Eledath, G. Medioni, and L. Sigal, "Energy-based learning for scene graph generation," in *Proceedings of the IEEE/CVF Conference on Computer Vision and Pattern Recognition*, 2021, pp. 13 936–13 945. 2

[59] K. Tang, Y. Niu, J. Huang, J. Shi, and H. Zhang, "Unbiased scene graph generation from biased training," in *Proceedings of the IEEE/CVF Conference on Computer Vision and Pattern Recognition*, 2020, pp. 3716–3725. 2, 6

[60] H. Liu, N. Yan, M. Mortazavi, and B. Bhanu, "Fully convolutional scene graph generation," in *Proceedings of the IEEE/CVF Conference on Computer Vision and Pattern Recognition*, 2021, pp. 11 546–11 556. 2, 6, 7

[61] B. Kim, J. Lee, J. Kang, E.-S. Kim, and H. J. Kim, "Hotr: End-to-end human-object interaction detection with transformers," in *Proceedings of the IEEE/CVF Conference on Computer Vision and Pattern Recognition*, 2021, pp. 74–83. 2, 3

[62] Y. Wang, Z. Xu, X. Wang, C. Shen, B. Cheng, H. Shen, and H. Xia, "End-to-end video instance segmentation with transformers," in *Proceedings of the IEEE/CVF Conference on Computer Vision and Pattern Recognition*, 2021, pp. 8741–8750. 2

[63] W. Liu, S. Chen, L. Guo, X. Zhu, and J. Liu, "Cptr: Full transformer network for image captioning," *arXiv preprint arXiv:2101.10804*, 2021. 2

[64] F. Zeng, B. Dong, T. Wang, C. Chen, X. Zhang, and Y. Wei, "Motr: End-to-end multiple-object tracking with transformer," *arXiv preprint arXiv:2105.03247*, 2021. 3

[65] X. Zhu, W. Su, L. Lu, B. Li, X. Wang, and J. Dai, "Deformable detr: Deformable transformers for end-to-end object detection," in *International Conference on Learning Representations (ICLR)*, 2021. 3, 5, 6

[66] Z. Yao, J. Ai, B. Li, and C. Zhang, "Efficient detr: Improving end-to-end object detector with dense prior," *arXiv preprint arXiv:2104.01318*, 2021. 3

[67] C. Zou, B. Wang, Y. Hu, J. Liu, Q. Wu, Y. Zhao, B. Li, C. Zhang, C. Zhang, Y. Wei *et al.*, "End-to-end human object interaction detection with hoi transformer," in *Proceedings of the IEEE/CVF Conference on Computer Vision and Pattern Recognition*, 2021, pp. 11 825–11 834. 3

[68] R. Stewart, M. Andriluka, and A. Y. Ng, "End-to-end people detection in crowded scenes," in *Proceedings of the IEEE conference on computer vision and pattern recognition*, 2016, pp. 2325–2333. 4

[69] H. Rezatofighi, N. Tsoi, J. Gwak, A. Sadeghian, I. Reid, and S. Savarese, "Generalized intersection over union: A metric and a loss for bounding box regression," in *Proceedings of the IEEE/CVF Conference on Computer Vision and Pattern Recognition*, 2019, pp. 658–666. 4, 5

[70] I. Loshchilov and F. Hutter, "Decoupled weight decay regularization," in *International Conference on Learning Representations (ICLR)*, 2019. 6

[71] R. Al-Rfou, D. Choe, N. Constant, M. Guo, and L. Jones, "Character-level language modeling with deeper self-attention," in *Proceedings of the AAAI Conference on Artificial Intelligence*, vol. 33, no. 01, 2019, pp. 3159–3166. 6